Detailed study on the role of oxygen vacancies in structural, magnetic and transport behavior of magnetic insulator: Co–CeO_2

2009 J. Phys.: Condens. Matter 21 486004

(http://iopscience.iop.org/0953-8984/21/48/486004)

J. Phys.: Condens. Matter **21** (2009) 486004 (9pp) doi:10.1088/0953-8984/21/48/486004

Detailed study on the role of oxygen vacancies in structural, magnetic and transport behavior of magnetic insulator: Co–CeO_2

Lubna R Shah[1,4], Bakhtyar Ali[2], Hao Zhu[1], W G Wang[1], Y Q Song[3], H W Zhang[3], S I Shah[1,2] and J Q Xiao[1,4]

[1] Physics and Astronomy, University of Delaware, Newark, DE 19716, USA
[2] Materials Science and Engineering, University of Delaware, Newark, DE 19716, USA
[3] School of Microelectronic and Solid-State Electronic, University of Electronic Science and Technology of China, Chengdu, 610054, People's Republic of China

E-mail: shah@udel.edu and jqx@udel.edu

Received 12 September 2009, in final form 19 October 2009
Published 11 November 2009
Online at stacks.iop.org/JPhysCM/21/486004

Abstract

Room temperature ferromagnetism in polycrystalline $Co_xCe_{1-x}O_{2-\delta}$ ($0.001 \leqslant x \leqslant 0.10$) bulk samples has been investigated. Annealing in the forming gas transformed the as-prepared paramagnetic into a ferromagnetic insulating material with over two orders of magnitude enhancement (from 3.7×10^{-2} to 1.24 μ_B/Co) in the magnetization. Structural characterization of both the as-prepared and H_2-treated samples showed a single phase material. The incorporation of Co with the formation of oxygen vacancies in the oxide lattice was revealed by x-ray photoelectron spectroscopy (XPS). The presence of oxygen vacancies is indicated by the existence of mixed valence states of cerium (Ce^{4+} and Ce^{3+}) in the high resolution XPS 3d spectrum. The role of the donor defects (oxygen vacancies) has been verified through the removal of oxygen vacancies. The ferromagnetic insulating ground state has been explained in terms of the interaction of the F^+ center and 3d magnetic cations. The connection between magnetic properties, electronic structure of the magnetic impurity and donor defect has been established. First principle calculations have been performed using the full potential linearized augmented plane wave method within the density functional theory (DFT) framework; these support our experimental findings. Both the experiment and calculations reinforced the crucial role of oxygen vacancies.

(Some figures in this article are in colour only in the electronic version)

1. Introduction

The development of materials with high Curie temperature (T_c) has spurred a tremendous interest in wide bandgap magnetic oxide semiconductors (OS). In order to understand the vital role of defects in mediating the ferromagnetic exchange, defects and their link to ferromagnetism (FM) has been the focus of recent research. Defects, in particular, oxygen vacancies (V_o), appear to be critical in understanding the FM in oxide semiconductors [1–4]. It has been proposed that V_o forming a donor impurity band can assist in establishing the FM exchange in OS including ZnO, TiO_2, and SnO_2 [5–7]. Beside the general semiconducting behavior some wide bandgap materials such as CeO_2 are found to be ferromagnetic dielectrics/insulators [8–10]. Therefore, the exchange mechanism behind the room temperature ferromagnetism (RTFM) in such materials is expected to differ from that in magnetic oxide semiconductors. Hence, systematic studies of the magnetic and transport properties in these magnetic dielectrics are needed in order to understand the mechanism responsible for ferromagnetic interactions.

[4] Authors to whom any correspondence should be addressed.

Table 1. Ferromagnetism in undoped and transition metal (Co, Ni)-doped CeO_2.

Dopant	Moment	Sample condition	Substrate	T_c (K)	Reference
Co ($x \leqslant 0.05$)	6.1 μ_B/Co	Films (PLD)	$LaAlO_3$(001)	725	[12]
None	1.9×10^{-3} emu g^{-1}	Nanoparticles (solid-state reaction)	—	—	[15]
Co ($x = 0.045$)	1.5 ± 0.2 μ_B/Co	Films (PLD)	SrTiO3(001) Si(001)	>400	[13]
Co ($x \leqslant 0.132$)	≈1 μ_B/Co	Films (electrochemical)	Si(001)	>350	[10]
Ni ($x \leqslant 0.04$)	0.1 μ_B/Ni	Nanoparticles (sol–gel)	—	~646	[16, 17]
Co ($x \leqslant 0.075$)	0.5 μ_B/Co	Nanoparticles (solid-state reaction)	—	>300	[18]
Co ($x \leqslant 0.125$)	5 μ_B/Co	Films (PLD)	Si(111) Al_2O_3(0001)	760	[19]
Ni ($x \leqslant 0.1$)	0.1 μ_B/Ni	Nanoparticles (sol–gel)	—	>300	[20]
Co ($x \leqslant 0.25$)	106 emu cm^{-3} for 25%	Films (PLD)	MgO(001) $SrTiO_3$(001)	>1000	[21]
None	0.023 μ_B/CeO_2	Nanoparticles (homogeneous precipitation)	—	>300	[22]
Co ($x \leqslant 0.10$)	1.24 μ_B/Co	Bulk (solid-state reaction)	—	>300	This work

CeO_2 is a transparent rare-earth oxide and a potential candidate as a magnetic insulator with several interesting properties such as: (1) a high dielectric constant ($\varepsilon = 26$) (2) a face-centered cubic (FCC) lattice with a fluorite crystal structure which is well matched with silicon (Si) (3) a very stable structure that can exist even with large off-stoichiometric oxygen, for example, $CeO_{2-\delta}$ ($0 \leqslant \delta \leqslant 0.5$) and (4) redox properties which can be widely used/studied in the field of catalysis [11–14].

An important aspect of CeO_2 was reported by Tiwari *et al* [12], showing that cobalt-doped CeO_2 is ferromagnetic with a high magnetic moment (8.2 μ_B/Co) and a high T_c (725 K). In this case the giant magnetic moment was attributed to the unquenched orbital magnetic moments of Co. Following this study, there have been a number of reports on the FM in various 3d transition metals (TM)-doped CeO_2 is summarized in table 1. Although in most of the papers, the F-center exchange mechanism (mediated through oxygen vacancies) is believed to be responsible for the FM, no clear correlation between ferromagnetism and conduction properties was established. In addition, none of these works presented any relationship between sub-bandgap levels of defects/magnetic dopant, magnetic and transport properties. Therefore, considering the potential role of V_o in FM exchange, it is important to carry out a detailed investigation on TM-doped CeO_2.

We have carried out a series of systemic experiments for the study of structural, magnetic, and transport properties of the as-prepared, as well as reduced (annealed in hydrogen, referred to as hydrogen-treated) samples. In addition, we have performed first principle calculations based on the density functional theory (DFT) that fully supports our experimental findings. Moreover, our results demonstrate that the presence of carriers through V_o enables magnetic percolation (not necessarily conductive percolation).

The correlation between the origin of ferromagnetism, conductivity, and the charge state of oxygen vacancies in the material has been described. It has been shown here that the magnetic properties of doped CeO_2 are more complex than previously reported. Finally, our adopted FM exchange mechanism in Co-doped CeO_2 is supported by a reverse experiment where we partially remove oxygen vacancies.

2. Experimental details

Polycrystalline bulk samples of $Co_xCe_{1-x}O_{2-\delta}$ ($0.001 \leqslant x \leqslant 0.10$) with oxygen vacancies (δ) were fabricated by the standard solid-state reaction method. Appropriate amounts of high purity CeO_2 (99.99%) and CoO (99.99%) powders were mixed thoroughly, palletized and calcined at 1300 °C for 10 h in air. The process of grinding, palletizing and calcining was repeated several times to ensure the uniform mixing of Co in $Ce_{1-x}Co_xO$ ($x = 0.001, 0.002, 0.01, 0.03, 0.06$ and 0.1) ceramic pellets. Annealing of the CeO_2 samples for each concentration of Co was done in the presence of a mixture of Ar (95%) and H_2 (5%) forming gas at 600 °C for 2 h (the samples are labeled as H_2-treated).

In order to characterize the structure x-ray diffraction (XRD) with Cu Kα radiation ($\lambda = 1.5405$ Å) was used. Scanning electron microscopy (SEM), energy dispersive x-ray (EDX) and x-ray photoelectron spectroscopy (XPS) were employed for compositional analyses. XPS was performed on samples with an SSI-M-probe equipped with an Al Kα monochromatic x-ray source and an energy resolution of ~0.1 eV. The base pressure in the XPS chamber was about 1×10^{-9} Torr prior to the start of data collection. In order to avoid any possibility of generating oxygen vacancies as a result of the high energetic x-rays, the spectra were collected right after exposing the sample to x-rays as described in the literature [23]. For charge neutralization, a 1 eV electron

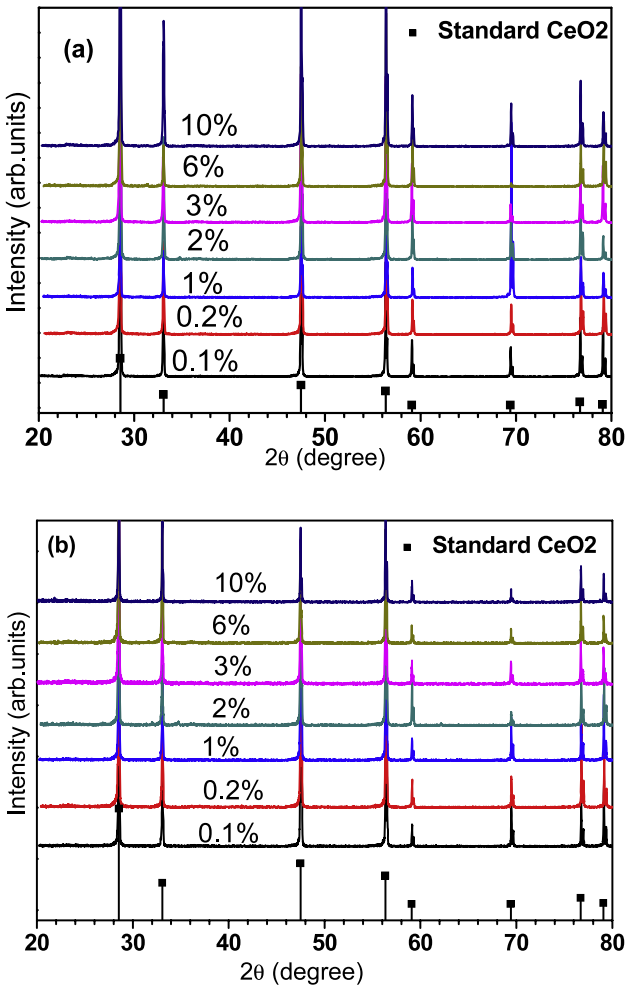

Figure 1. X-ray diffraction patterns of bulk $Co_xCe_{1-x}O_{2-\delta}$ samples with various concentrations of cobalt (Co): (a) the as-prepared, (b) the H_2-treated samples.

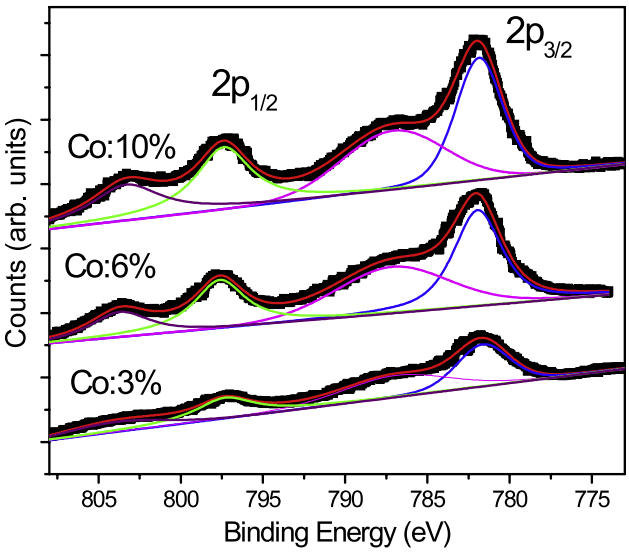

Figure 2. XPS spectra of the Co 2p region for the as-prepared $Co_xCe_{1-x}O_{2-\delta}$ samples with $x = 3\%$, 6% and 10%.

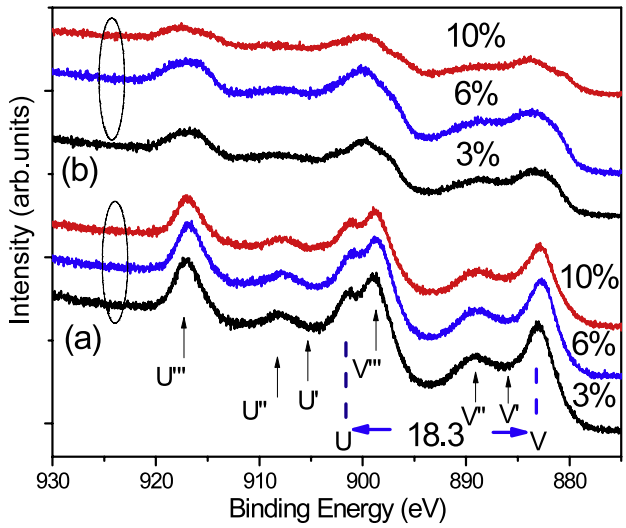

Figure 3. X-ray photoelectron spectroscopy spectra of the Ce 3d region of $Co_xCe_{1-x}O_{2-\delta}$ samples with $x = 3\%$, 6% and 10%: (a) as-prepared, (b) H_2-treated.

beam was used. A pass energy of 50 eV and an x-ray power of 100 W were employed. The charge correction was done using the carbon 1s peak (binding energy = 284.6 eV) as the reference. Magnetic measurements were carried out with a vibrating sample magnetometer (VSM, Lake Shore). Transport properties were measured using a standard four-probe technique.

3. Results and discussion

X-ray diffraction analyses of the as-prepared and the H_2-treated samples indicate that all the samples with $x \leqslant 0.1$ are single phase and have the same fluorite structure of CeO_2. None of the samples in our compositional range of $x \leqslant 0.1$ showed any evidence of impurity phases. This shows that H_2 treatment has no effect on the structure of the Co–CeO_2 matrix. The XRD data of the as-prepared and H_2-treated samples is shown in figures 1(a) and (b).

A detailed study of the XPS spectra of Co 2p and Ce 3d regions has been performed to identify the oxidation states of Co and Ce ions. In addition, oxygen (O) 1s regions are used to obtain the information on the presence/absence of oxygen vacancies (V_o). Co 2p spectra, displayed in figure 2, show that all samples have four peaks: $2p_{3/2}$, $2p_{1/2}$ doublet, and their corresponding shake-ups (satellites). The obtained binding energies for Co $2p_{3/2}$ (781.9 eV) and $2p_{1/2}$ (797.4 eV) are close to those reported for Co^{2+} ions in Co–O bonding with an energy difference between Co $2p_{3/2}$ and Co $2p_{1/2}$ of 15.5 ± 0.1 eV [24]. This is an excellent match with the reported energy difference for Co surrounded by O atoms in the tetrahedral symmetry (15.5 eV), whereas the energy difference for metallic cobalt is 15.05 eV [24]. Our XPS spectra of the Co 2p region suggest that Co is in a 2+ formal oxidation state.

The oxidation states of Ce can be determined by analyzing the Ce 3d spectra, shown in figure 3. These spectra exhibit clear differences between the as-prepared (figure 3(a)) and H_2-treated (figure 3(b)) samples. The differences appear to be due

Table 2. Information of the cerium 3d spectrum of x-ray photoelectron spectroscopy [26].

Peak label	Ce contribution	Peak position (eV)	Peak characteristics	Final state
U	Ce(IV)	901.0	$3d_{3/2}$	$Ce(3d^94f^2)O2p^4$
V	Ce(IV)	882.3	$3d_{5/2}$	
U″	Ce(IV)	907.5	$3d_{3/2}$	$Ce(3d^94f^1)O2p^5$
V″	Ce(IV)	888.9	$3d_{5/2}$	
U‴	Ce(IV)	916.8	$3d_{3/2}$	$Ce(3d^94f^0)O2p^6$
V‴	Ce(IV)	898.2	$3d_{5/2}$	
U^0	Ce(III)	880.5	$3d_{3/2}$	$Ce(3d^94f^1)O2p^6$
V^0	Ce(III)	898.8	$3d_{5/2}$	
U′	Ce(III)	904.2	$3d_{3/2}$	$Ce(3d^94f^1)O2p^5$
V′	Ce(III)	885.9	$3d_{5/2}$	

to the presence of Ce^{4+} and Ce^{3+} ions. Literature indicates that the Ce 3d spectrum can be fully described by five spin–orbit doublets ($3d_{5/2}$ and $3d_{3/2}$) [25]. The multiplicity of these states arises from different Ce 4f level occupancies in the final state. In the absence of defects, $Co_xCe_{1-x}O_{2-\delta}$ samples are expected to contain only the Ce^{4+} ions. The Ce 3d spectrum of Ce(IV) oxide shows three pairs of doublets shown in table 2 (U/V, U″/V″ and U‴/V‴). The labels follow the convention established by Burroughs *et al* [25]. The highest binding energy peaks, U‴ and V‴ arise from a $Ce(3d^9)$ $O(2p^6)$ $Ce(4f^0)$ final state [26]. The lower binding energy states, U″ and V″ arise from the final state $Ce(3d^9)$ $O(2p^5)$ $Ce(4f^1)$, and the doublet U and V from the final state $Ce(3d^9)$ $O(2p^4)$ $Ce(4f^2)$. In the case of Ce(IV) oxide, V and U spin–orbit splitting is 18.3 eV [27], whereas in the case of Ce(III) oxide, Ce 3d spectrum consists of two pairs of doublets (U^0, V^0, U′ and V′). Similar to the case of Ce^{4+}, the doublets U^0/V^0 and U′/V′ correspond to the final state $Ce(3d^9)$ $O(2p^6)$ $Ce(4f^1)$ and $Ce(3d^9)$ $O(2p^5)$ $Ce(4f^2)$, respectively.

From the above discussion, the spectral features, characteristic of either Ce^{4+} or Ce^{3+}, can be used to identify the presence of these species in our samples. It is obvious from the spectra that both the as-prepared (figure 3(a)) and the H_2-treated (figure 3(b)) samples exhibit the distinctive features of Ce^{4+}, namely, the presence of U‴ peak as well as the V and U splitting of 18.3 eV. In addition there are some weaker features of U′ and V′ indicating the presence of Ce^{3+}, especially in samples containing higher Co concentrations. The presence of the Ce^{3+} can be explained by the substitution of Ce^{4+} ions by Co^{2+} ions. During this, oxygen vacancies may arise to maintain the charge neutrality when Ce^{4+} reduces to Ce^{3+}. The presence of the doublet (U′ and V′) due to Ce^{3+} is more prominent in H_2-treated samples, which demonstrates that H_2 treatment favors the reduction of Ce^{4+} to Ce^{3+}. This is accompanied by the formation of oxygen vacancies ($2Ce^{4+}{}_{Lattice} + 4O^{2-}{}_{Lattice} \rightarrow V_o + O + 2Ce^{3+}{}_{Lattice} + 3O^{2-}{}_{Lattice}$) [28]. Hence the XPS results conclude that a high concentration of oxygen vacancies is present in the H_2-treated samples.

In addition to the high resolution spectra of Co and Ce, figure 4 shows the O 1s core level spectra for the as-prepared ($x = 0.03, 0.06$ and 0.1) and H_2-treated ($x = 0.03$ and 0.1) $Co_xCe_{1-x}O_{2-\delta}$ samples. It is important to note that all

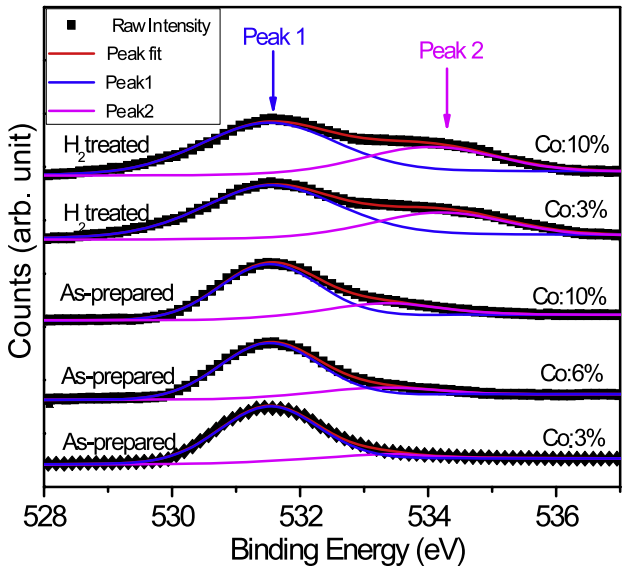

Figure 4. X-ray photoelectron spectroscopy core level spectra of O 1s for the as-prepared and the H_2-treated $Co_xCe_{1-x}O_{2-\delta}$ samples with $x = 3\%$, 6% and 10%. Peak 1 and peak 2 correspond to Ce^{4+}–O and Ce^{3+}–O contributions, respectively.

the samples were collectively loaded in the XPS chamber for data collection under the same conditions. Analysis of the O 1s XPS spectra for the as-prepared samples shows a slightly asymmetric peak, which can be fitted by two Gaussian peaks. The de-convoluted peak at a lower binding energy is labeled as peak 1, whereas the peak at a higher binding energy is labeled as peak 2. In the as-prepared samples, the asymmetry associated with the O 1s peak increases with increasing Co concentrations in the samples. This increase becomes remarkably pronounced in the H_2-treated samples. Furthermore, a close examination of the relative areas of peak 2 and peak 1 (shown in figure 5) exhibits an interesting feature where the ratio of the area of the peaks (peak 2/peak 1) increases as the Co concentration increases or samples are H_2-treated. This trend appears to be due to the creation of oxygen vacancies as a result of non-isovalent dopant or annealing in H_2 environment.

It is worth mentioning that there is a controversy in the interpretation of O 1s XPS spectra for oxides such as TiO_2, ZnO, and CeO_2. There are reports, which indicate that the high binding energy peak arises from hydroxyl groups OH, or other radicals on the sample surface such as CO, or CO_2 [26, 29, 30]. However, the high binding energy peak in an O1s spectrum could also be related to the presence of V_o [31, 32]. In our case with increasing Co concentration as well as H_2 treatment, there is a systematic increase in the high binding energy component of the O 1s spectrum. This feature is accompanied by an increase of Ce^{3+} ions, a peak (V′), and a decrease of Ce^{4+} ions whose characteristic peak is U‴. Thus the analysis of the Ce 3d spectrum reveals that oxygen vacancies are accompanied with Ce^{4+} reducing to Ce^{3+}, which is consistent with the evolution of the high binding energy peak in the O 1s core level spectra. The existence of the peak at a higher binding energy can be explained as 1s electrons in oxygen are more tightly bonded to

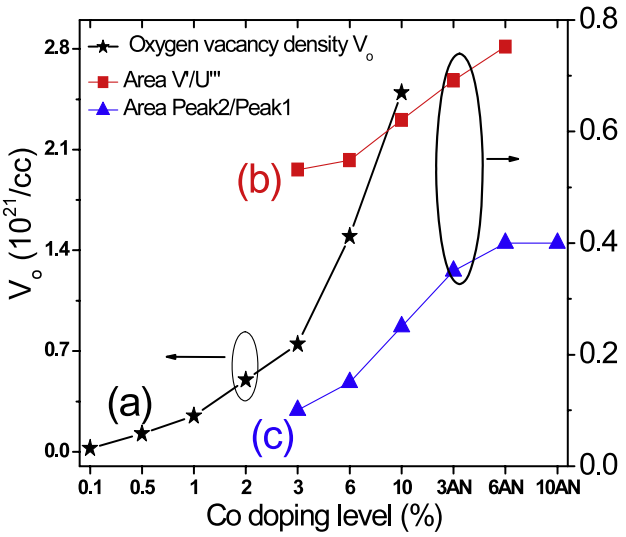

Figure 5. (a) Co concentration-dependent oxygen vacancy density (V_o) calculated from charge neutrality requirement (Co^{2+} substitute for Ce^{4+} in CeO_2). (b) Relative areas of peak V′ and U‴ (from Ce 3d XPS) and (c) peak 2 and peak 1 (from O 1s XPS) are also plotted (red and blue points). Note: 3AN, 6AN and 10AN corresponds to H_2-treated Co–CeO_2 samples with $x = 3\%$, 6% and 10%, respectively.

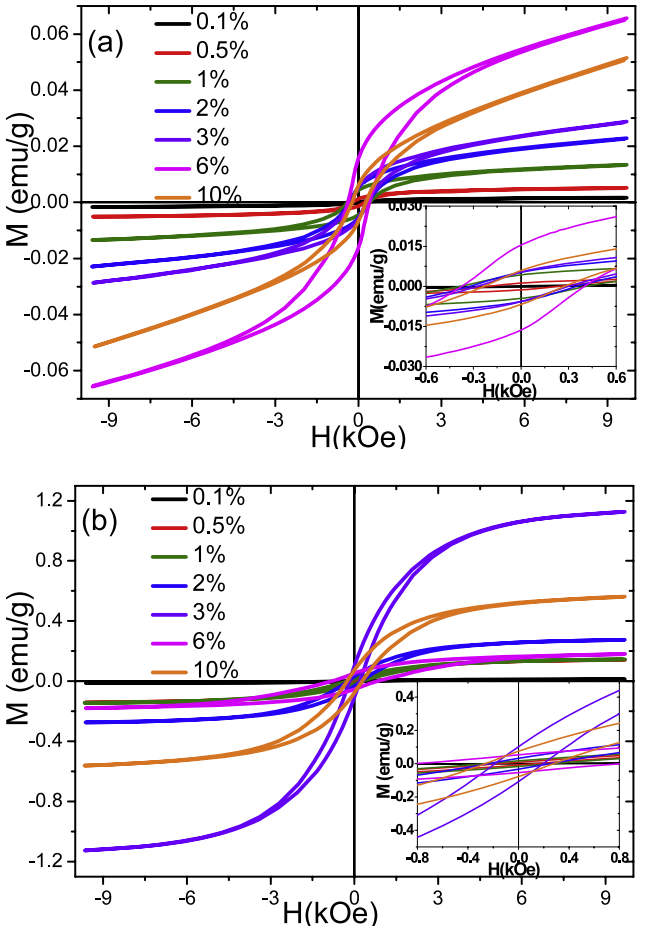

Figure 6. Magnetic hysteresis curves for (a) as-prepared and (b) H_2-treated $Co_xCe_{1-x}O_{2-\delta}$ samples with various Co concentrations. Insets: the magnified version of the same data at low fields.

oxygen in the case of the 3+ oxidation state of cerium (O–Ce^{3+} bond), as compared to cerium in the 4+ state (O–Ce^{4+} bond). Based on the above discussion it is clear that the asymmetry in the O 1s spectrum is related to the presence of oxygen vacancies. In addition, figure 5 includes the oxygen vacancies calculated from the charge neutrality condition as well as from the relative area of V′ and U″, which is an indirect way to show the presence of the oxygen vacancy density through the signature of Ce^{3+} in the Ce 3d spectrum. Hence, the presence of oxygen vacancies is confirmed by analysis of both by the Ce 3d and the O 1s core level spectra.

Having confirmed the presence of oxygen vacancies, it is important to understand how the magnetic and transport behaviors are affected by these vacancies in Co–CeO_2. To this end, we studied the magnetic hysteresis curves of the pure CeO_2 and Co–CeO_2 in the as-prepared and H_2-treated conditions. Pure CeO_2 samples in both the as-prepared and the H_2-treated condition are observed to be paramagnetic (PM) whereas Co–CeO_2 samples under the same treatment show ferromagnetic behavior for all Co concentrations. Magnetic hysteresis (MH) loops of the as-prepared and H_2-treated $Co_xCe_{1-x}O_{2-\delta}$ samples are shown in figures 6(a) and (b). To quantify the magnetic parameters including ferromagnetic saturation magnetization M_{FM}^{S}, remanence M_{FM}^{R}, and intrinsic coercivity H_{ci}, we used the following fitting function, made up of FM and PM parts [33]:

$$M(H) = 2\frac{M_{FM}^{S}}{\pi}\tan^{-1}\left[\frac{H \pm H_{ci}}{H_{ci}}\tan\left\{\frac{\pi M_{FM}^{R}}{2M_{FM}^{S}}\right\}\right] + \chi H.$$

The first term is a ferromagnetic (FM) hysteresis curve and the second represents a possible paramagnetic (PM) contribution. The parameters obtained for $Co_xCe_{1-x}O_{2-\delta}$ as-prepared and H_2-treated samples are summarized in figure 7.

Interestingly, even for 0.1% Co concentration, the as-prepared sample shows room temperature ferromagnetism with a magnetic moment of 3.7×10^{-2} μ_B/Co and coercivity of about 208 Oe. The magnetization is observed to increase with increasing Co concentration. It is important to mention that although the magnetization of the samples increases with increasing Co concentration in the sample, the magnetic moment per Co atom decreases. Moreover, there is an increase of over an order in magnetization of the samples with H_2 treatment. However, there is no clear trend in the magnetic moment per Co (μ_B/Co) with Co concentration in the H_2-treated samples (figure 7(c)). The maximum value of magnetization observed is 1.24 μ_B/Co for H_2-treated samples with 3% Co-doping. To examine the room temperature ferromagnetism in Co–CeO_2, we consider four possible types of magnetic states for Co in the CeO_2 matrix: (a) FM exchange coupling; (b) FM Co clusters; (c) isolated PM Co due to small doping concentrations; (d) antiferromagnetic (AFM) exchange coupling between Co atoms through oxygen.

In order to check for the presence/absence of metallic Co clusters, we assume that the observed FM is due to the embedded Co clustering effect. In this scenario, if we consider the magnetic moment of metallic Co, which is 1.72 μ_B/Co,

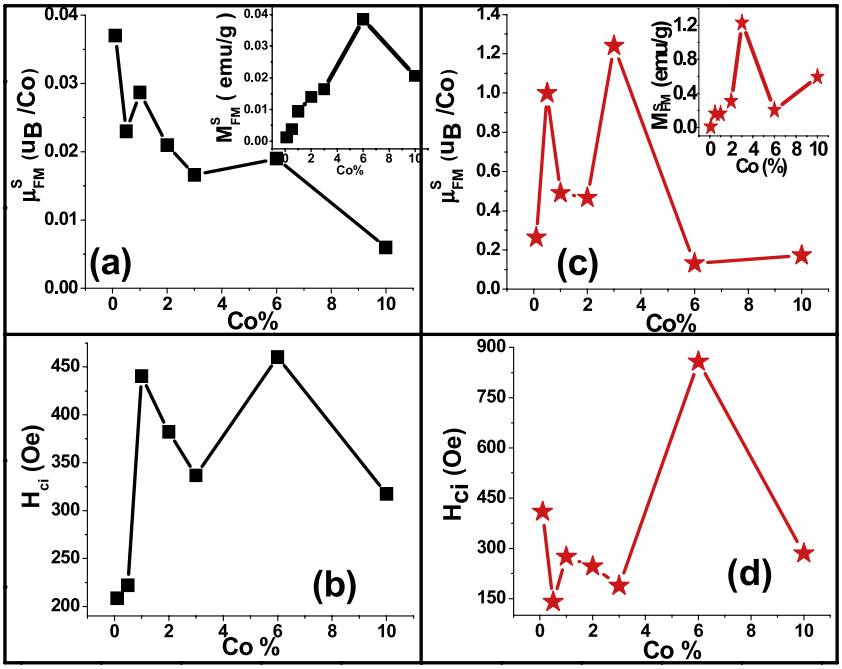

Figure 7. Values of the intrinsic coercivity and magnetic moment obtained from MH loops for the as-prepared ((a), (b)) and the H_2-treated ((c), (d)) $Ce_{1-x}Co_xO_2$ samples as a function of Co concentration. Insets show magnetization (emu g^{-1}) versus Co concentration.

one can estimate the amount of Co clusters in the samples [34]. Based on such calculations, about 70% of the doped Co has to form clusters to give the observed moment 1.24 μ_B/Co. This large fraction of the substituted Co in cluster form is more than enough to show up in the XPS 2p spectrum of Co. However, there is no indication of metallic Co in the XPS data. Hence, it is clear that in our Co–CeO_2 samples the observed FM signal is not due to Co clusters. Furthermore, the enhancement in FM as a result of annealing the as-prepared samples in H_2 environment can be attributed to the creation of oxygen vacancies. It appears that there might be a bigger fraction of isolated Co ions unable to interact via exchange coupling with each other and remaining in the paramagnetic state. When samples are H_2-treated, an increase in the defect (V_o) density is expected, which gives rise to FM coupling among the isolated Co atoms.

The key issue here is to understand the role of oxygen vacancies in the FM in Co–CeO_2. The exchange mechanisms that could establish the ferromagnetism are Ruderman–Kittel–Kasuya–Yosida (RKKY) interactions and/or bound magnetic polarons (BMP) [5]. The former requires a metallic system whereas the latter can exist in semiconducting/insulating materials. Taking into account the existence of oxygen vacancies in our system, we consider the FM exchange mechanism further rather than interpreting the behaviors with the usual BMP theory. There is a sub category of BMP theory named F-center exchange (FCE) [5, 7]. This candidate mechanism has been applied to explain the room temperature FM in magnetic insulators, e.g. TiO_2 and SnO_2.

The F-center exchange (FCE) mechanism deals in depth with the FM arising due to the presence of oxygen vacancies. There are three possible charge states of an oxygen vacancy: (a) F^{2+} center with no trapped electrons; (b) F^+ center with one trapped electron and (c) F^0 center with two trapped electrons. The F^0 center charge states are in a singlet ($S = 0$) state and form a shallow donor level or lie above the conduction band edge. This can only mediate weak AFM exchange between magnetic dopants. In some cases, the impurity band which is formed due to the F^0 center states when the overlap with the conduction band of the host oxide (4s band), it favors the FM [5] but its strength is very weak. In contrast to this, singly occupied vacancies (F^+ center) lie deep in the gap and favor a FM ground state as shown in figure 8.

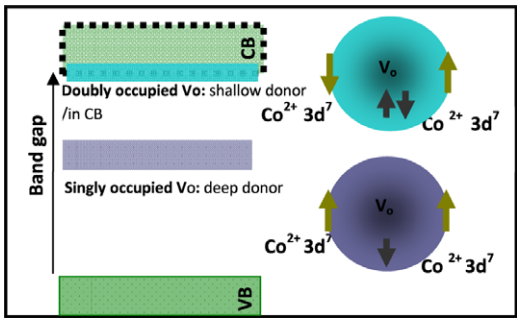

Figure 8. Schematic representation of the F-center exchange due to singly and doubly occupied oxygen vacancies. The corresponding defect levels in the bandgap of CeO_2 are also shown.

The transport behavior of the material was considered to further investigate the underlying mechanism in the FM coupling in $Co_xCe_{1-x}O_{2-\delta}$. To this effect the resistivity of the samples was measured using the four-probe technique. All the as-prepared $Co_xCe_{1-x}O_{2-\delta}$ samples have very high resistivity at room temperature, above the measurement limit of the setup (10^6 Ω cm). This suggests a very small carrier concentration in

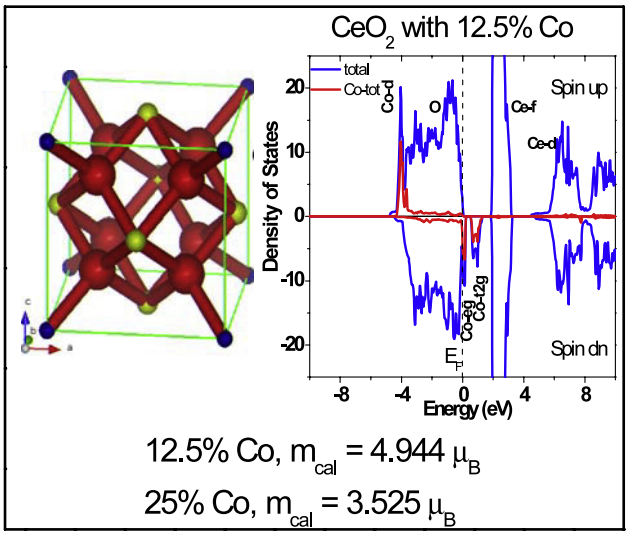

Figure 9. Structure of the $Co_xCe_{1-x}O_{2-\delta}$ system and the calculated density of states for the sample with $x = 12.5\%$. Solid red (large balls), blue (small balls at the corners), green (small balls) correspond to O, Co and Ce atoms, respectively.

the as-prepared samples, not capable of establishing the long range FM coupling among Co atoms. This insulating state, with resistivity greater than 10^6 Ω cm, persists in the samples even after H_2-treatment. Therefore, itinerant FM exchange is not valid in this case.

To correlate the magnetic and transport behaviors of the samples, the F^+ center is the underlying mechanism in establishing the FM state. As discussed earlier, electrons in these singly occupied oxygen vacancies (F^+) are strongly localized. The localization radius is $\varepsilon(m/m^*)a_0$, where ε is the dielectric constant, m and m^* are the mass and effective mass of an electron with a_0 as the Bohr radius [5]. Thus the estimated value for the F-electron orbital in CeO_2 ($\varepsilon = 26$) is about 46 Å. This explains the smaller magnetic moment in the as-prepared samples. That is, at low Co concentrations, the magnetic dopants are far apart and cannot be coupled through F^+ centers, resulting in small magnetization in the as-prepared samples (6×10^{-3}–3.7×10^{-2} μ_B/Co). Contrary to the as-prepared samples, in the H_2-treated samples, enough V_o is created (preferentially near Co ions) to form the F^+ center, which is capable of mediating strong FM coupling. The critical F^+ center density (n_{vo}) required for a long range FM order can be estimated to be $\gamma^3\delta_p = n_{vo}/n_o \approx 4.3$ [5], where $\gamma = \varepsilon(m/m^*)$ and n_o is the oxygen density (5×10^{28} m^{-3}) in CeO_2. In the present case, using $\varepsilon = 26$ and $m^*/m = 0.3$ for CeO_2 with a fluorite structure, n_{vo} is calculated to be $\approx 3 \times 10^{23}$ m^{-3}. Once the F^+ center density reaches this critical value for magnetic percolation, these F^+ centers overlap, which results in the spin polarization of the majority of Co ions. This leads to an increase in the magnetization in H_2-treated samples (figure 7(c)). Thus, it seems very likely that doped magnetic impurities (Co) in CeO_2 form relatively deep levels in the CeO_2 bandgap. Furthermore, these deep lying energy levels of Co might energetically align with the defect level (F^+ center) and lead to a long range ferromagnetic ordering even in the absence of itinerant carriers.

We performed first principle calculations in order to support the experimental results. The calculations were carried out using the full potential linearized augmented plane wave method [35] and the generalized gradient approximation within the density functional theory (DFT) framework [36, 37]. Details of the calculations will be reported elsewhere [38]. Our calculations show that in pure CeO_2, the oxygen vacancy

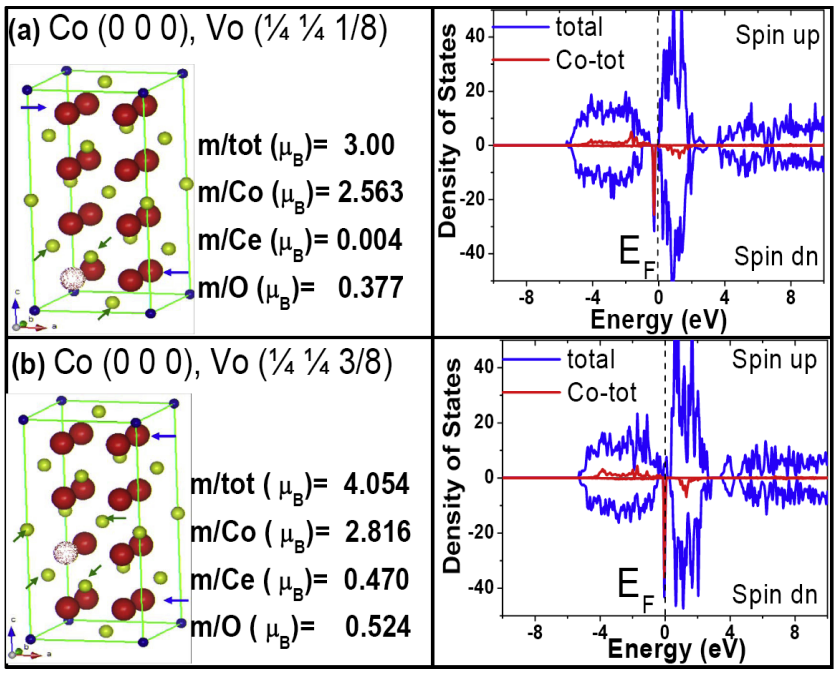

Figure 10. Structures for 12.5% Co and 6.25% oxygen vacancies in CeO_2. The specific positions of the oxygen vacancy are at (1/4, 1/4, 1/8) and (1/4, 1/4, 3/8) for (a) and (b), respectively. The solid red (large balls), blue (small balls at the corners), green (small balls), and dotted red represent O, Co, Ce, and oxygen vacancies (V_o), respectively. The calculated density of states for a given structure is also displayed.

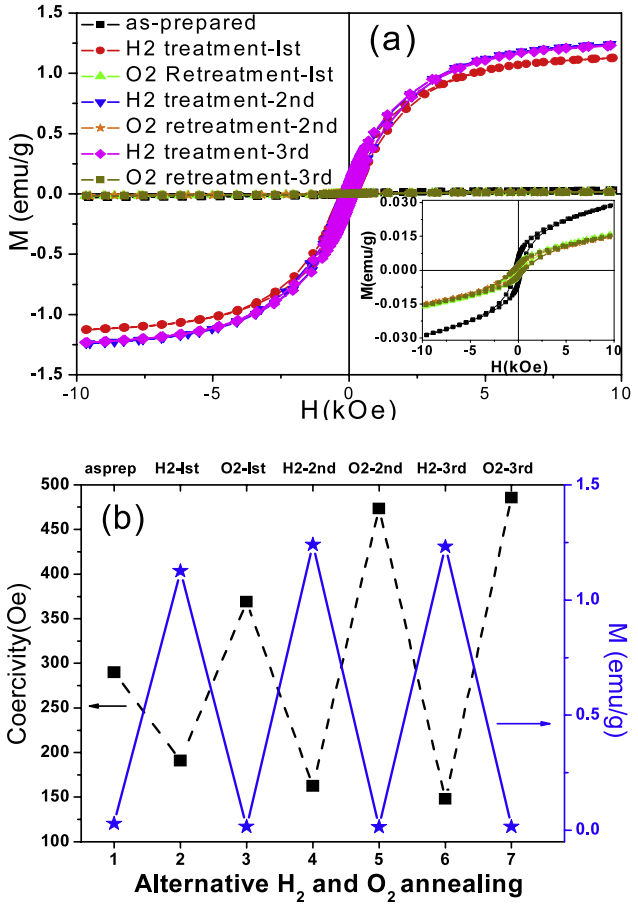

Figure 11. (a) Magnetization hysteresis loops for bulk $Co_xCe_{1-x}O_{2-\delta}$ samples for alternative H_2 and O_2 annealing. For clarity purposes, as-prepared and all O_2 re-treated loops are shown again in the inset. (b) Coercivity and magnetization values for alternating H_2 and O_2 annealing.

pulls the d and f orbits of Ce closer to the Fermi level, causing exchange splitting, but due to the small density of states at the Fermi level, only the oxygen vacancy itself cannot induce an obvious FM in pure CeO_2.

On the other hand, in $Co_xCe_{1-x}O_{2-\delta}$, besides spin-polarized Co in a high spin state, the substituted Co also effectively spin-polarizes the neighboring Ce and O atoms. The calculated density of states (DOS) for 12.5% Co-doped CeO_2 is shown in figure 9. The DOS around the Fermi level are determined by p orbitals of O, d orbitals of Co, and d and f orbitals of Ce. Parts of the d and f orbitals of Ce are occupied as they cross the Fermi level. This suggests that Co–CeO_2 is ferromagnetically stable. The study of the electronic structures and magnetic properties for 25% and 12.5% Co-doped CeO_2 illustrate that, at 12.5%Co concentration, the nearest neighbor (NN) O atoms will be more effectively spin-polarized, and the next NN Ce atoms also tend to be polarized indirectly by Co via O. Furthermore, the calculated magnetic moments of CeO_2 with a varied Co content are qualitatively in accordance with the experimental trends shown in figure 7(a), i.e., at lower Co concentrations, O atoms neighboring a Co atom are more effectively spin-polarized, thus causing larger magnetic moments, leading to an inverse correlation between saturation moments and Co contents.

Next we considered the coexistence of magnetic dopant (Co) and oxygen vacancies in CeO_2. To clarify the role of oxygen vacancies in spin-polarization of the neighboring Ce, the Co content and oxygen vacancies are fixed at 12.5% and 6.25%, respectively, but the specific position of the oxygen vacancy (V_o) is varied in figure 10 as in case 1 (V_o and Co as NN) and case 2 (V_o and Co are not NN). The corresponding total DOS and partial DOS for Co are shown in figure 10. With the same amount of oxygen vacancy, the moment contributed by Co, Ce and O in case 1 are smaller than in case 2, which results in different overall magnetic moments in these two cases. This strong dependence of total magnetic moment on the local electronic environment of magnetic dopant (Co) can also be used to explain the randomness of saturation magnetization with variations of Co-doping for hydrogen-treated $Co_xCe_{1-x}O_{2-\delta}$ samples (figure 7(c)), though this assumption needs further investigations.

Finally, in order to check the validity of FCE mechanisms, we performed a *reverse experiment* by annealing the H_2-treated samples in an O_2 atmosphere. We expected that the change in the F^+ center density would significantly affect the magnetic behavior. Magnetization hysteresis loops corresponding to alternative H_2- and O_2-treatment are plotted in figure 11(a), whereas the inset shows the MH loops for the as-prepared and the O_2-re-treated samples. Samples treated first in H_2 show strong ferromagnetism. The second O_2-treatment, which is expected to decrease the oxygen vacancy density, suppresses the ferromagnetism. By re-introducing F^+ centers through a second H_2-treatment, a strong ferromagnetism is achieved again.

It is noteworthy that after the first H_2-treatment, O_2-re-treatment does not recover the as-prepared state, rather it leads to a lower magnetization than of that in the as-prepared samples. However, further alternating H_2- and O_2-treatments are completely reversible, i.e. the magnetic properties are the same in O_2 (H_2) treated samples regardless of its treatment sequence. This observation illustrates that the as-prepared state had some donor defects in addition to oxygen vacancies due to charge neutrality condition. These native defects and oxygen vacancies created due to H_2-treatment are compensated in O_2 annealing. But the presence of Co^{2+} in Ce^{4+} site prevents the complete removal of oxygen vacancies and its associated ferromagnetism. Therefore, after the first cycle of O_2 treatment, the sample can be switched back and forth with alternative H_2 and O_2 annealing. Figure 11(b) shows the magnetization and coercivity values extracted from the magnetization loops, respectively.

4. Conclusion

We have systematically studied the structural, transport and magnetic behaviors of $Co_xCe_{1-x}O_{2-\delta}$ ($x = 0.001, 0.005,$ 0.01, 0.02, 0.03, 0.06 and 0.10, δ = oxygen vacancies) samples. Structural analyses of the x-ray diffraction data indicate that all the samples are single phase with no indication of Co metal or Co oxides. X-ray photoelectron spectroscopy of cobalt show that Co is in the form of Co^{2+} and is incorporated in the host oxide matrix. The presence of oxygen vacancies

are corroborated through the XPS analyses of the 3d spectra of cerium for $Co_xCe_{1-x}O_{2-\delta}$ samples, which also shows that Ce^{4+} reduces to Ce^{3+}, either with Co-doping or annealing in the forming gas. Our experiments indicate that all the doped samples exhibit a room temperature ferromagnetic insulating ground state. Furthermore, the experimental and first principle calculations show that ferromagnetism is intimately linked with oxygen vacancies which help enhance the FM coupling of the Ce, as well as the doped magnetic impurity spins. For the ferromagnetic ground state, the F^+ center ferromagnetic exchange mechanism, which involves a spin-polarized electron trapped at an oxygen vacancy, is suggested. Our proposed ferromagnetic exchange mechanism in $Co_xCe_{1-x}O_{2-\delta}$ samples is successfully supported by a reverse experiment as well as the electronic structure of the carrier associated with the defect (F^+ center) and magnetic impurity (Co).

Acknowledgments

This work is supported by the National Basic Research Program (973) under Grant No. 2007CB31407 and the International S&T Cooperation Program of China under Grant No. 2006DFA53410.

References

[1] Shah L R, Wang W, Zhu H, Ali B, Song Y Q, Zhang H W, Shah S I and Xiao J Q 2009 *J. Appl. Phys.* **105** 07C515
[2] Rahman G, Garcia-Suarez V M and Hong S C 2008 *Phys. Rev.* B **78** 184404
[3] Sudakar C, Kharel P, Lawes G, Suryanarayanan R, Naik R and Naik V M 2007 *J. Phys.: Condens. Matter* **19** 026212
[4] Guan L X, Tao J G, Xiao Z R, Zhao B C, Fan X F, Huan C H A, Kuo J L and Wang L 2009 *Phys. Rev.* B **79** 184412
[5] Coey J M D, Venkatesan M and Fitzgerald C B 2005 *Nat. Mater.* **4** 173
Ali B, Shah L R, Ni C, Xiao J Q and Shah S I 2009 *J. Phys.: Condens. Matter* **21** 456005
Ali B, Rumaiz A K, Ozbay A, Nowak E R and Shah S I 2009 *Solid State Commun.* **149** 2210
[6] Kittilstved K R, Liu W K and Gamelin D R 2006 *Nat. Mater.* **5** 291
[7] Fitzgerald C B, Venkatesan M, Dorneles L S, Gunning R, Stamenov P, Coey J M D, Stampe P A, Kennedy R J, Moreira E C and Sias U S 2006 *Phys. Rev.* B **74** 115307
[8] Fernandes V, Klein J J, Mattoso N, Mosca D H, Silveira E, Ribeiro E, Schreiner W H, Varalda J and de Oliveira A J A 2007 *Phys. Rev.* B **75** 121304
[9] Vodungbo B, Zheng Y, Vidal F, Demaille D, Etgens V H and Mosca D H 2007 *Appl. Phys. Lett.* **90** 062510
[10] Fernandes V, Klein J J, Mattoso N, Mosca D H, Silveira E, Ribeiro E, Schreiner W H, Varalda J and Oliveira A J A d 2007 *Phys. Rev.* B **75** 121304
[11] Shiau C-Y, Ma M W and Chuang C S 2006 *Appl. Catal.* A **301** 89
[12] Tiwari A, Bhosle V M, Ramachandran S, Sudhakar N, Narayan J, Budak S and Gupta A 2006 *Appl. Phys. Lett.* **88** 142511
[13] Vodungbo B, Vidal F, Zheng Y, Marangolo M, Demaille D, Etgens V H, Varalda J, Oliveira A J A d, Maccherozzi F and Panaccione G 2008 *J. Phys.: Condens. Matter* **20** 125222
[14] Guo Q, Wu M, Liu Y and Bai X 2007 *Chin. J. Catal.* **28** 953
[15] Sundaresan A, Bhargavi R, Rangarajan N, Siddesh U and Rao C N R 2006 *Phys. Rev.* B **74** 161306
[16] Thurber A, Reddy K M and Punnoose A 2007 *J. Appl. Phys.* **101** 09N506
[17] Thurber A, Reddy K M, Shutthanandan V, Engelhard M H, Wang C, Hays J and Punnoose A 2007 *Phys. Rev.* B **76** 165206
[18] Wen Q-Y, Zhang H-W, Song Y-Q, Yang Q-H, Zhu H and Xiao J Q 2007 *J. Phys.: Condens. Matter* **19** 246205
[19] Song Y Q, Zhang H W, Wen Q Y, Zhu H and Xiao J Q 2007 *J. Appl. Phys.* **102** 043912
[20] Misra S K, Andronenko S I, Engelhard M H, Thurber A, Reddy K M and Punnoose A 2008 *J. Appl. Phys.* **103** 07D122
[21] Bi L, Kim H-S, Dionne G F, Speakman S A, Bono D and Ross C A 2008 *J. Appl. Phys.* **103** 07D138
[22] Liu Y, Lockman Z, Aziz A and MacManus-Driscoll J 2008 *J. Phys.: Condens. Matter* **20** 165201
[23] Engelhard M, Azad S, Peden C H F and Thevuthasan S 2004 *Surf. Sci. Spectrosc.* **11** 73
[24] Wagner C D, Riggs W M, Davis L E and Moulder J F 1979 *Handbook of X-Ray Photoelectron Spectroscopy* (Eden Prairie, MN: Perkin-Elmer) p 78
[25] Burroughs P, Hamnett A, Orchard A F and Thornton G 1976 *J. Chem. Soc. Dalton Trans.* **17** 1686
[26] Mullins D R, Overbury S H and Huntley D R 1998 *Surf. Sci.* **409** 307
[27] Wang A Q and Golden T D 2003 *J. Electrochem. Soc.* **150** C616
[28] Qiu L, Liu F, Zhao L, Ma Y and Yao J 2006 *Appl. Surf. Sci.* **252** 4931
[29] Schierbaum K-D 1998 *Surf. Sci.* **399** 29
[30] El Fallah J, Hilaire L, Roméo M and Le Normand F 1995 *J. Electron Spectrosc. Relat. Phenom.* **73** 89
[31] Naeem M, Hasanain S K, Kobayashi M, Ishida Y, Fujimori A, Buzby S and Shah S I 2006 *Nanotechnology* **17** 2675
[32] Wang A Q, Punchaipetch P, Wallace R M and Golden T D 2003 *J. Vac. Sci. Technol.* B **21** 1169
[33] Duhalde S, Vignolo M F, Golmar F, Chiliotte C, Torres C E R, Errico L A, Cabrera A F, Rentería M, Sánchez F H and Weissmann M 2005 *Phys. Rev.* B **72** 161313
[34] Chambers S A, Heald S M and Droubay T 2003 *Phys. Rev.* B **67** 100401
[35] Blaha K S P and al G K H M e 2004 *Computer Code WIEN2k* Vienna Universtiy of Technology, Vienna, Austria
[36] Hohenberg P and Kohn W 1964 *Phys. Rev.* **136** B864
[37] Perdew J P, Burke K and Ernzerhof M 1996 *Phys. Rev. Lett.* **77** 3865
[38] Zhu H, Wen Q Y, Zhang H W and Xiao J Q 2009 *Phys. Rev.* B submitted